Journal of Sound and Vibration 329 (2010) 1875–1889

Contents lists available at ScienceDirect

Journal of Sound and Vibration

journal homepage: www.elsevier.com/locate/jsvi

Vibrations of carbon nanotube-reinforced composites

Giovanni Formica [a], Walter Lacarbonara [b,*], Roberto Alessi [b]

[a] Dipartimento di Strutture, Università degli Studi Roma Tre, 00146 Rome, Italy
[b] Dipartimento di Ingegneria Strutturale e Geotecnica, Università degli Studi di Roma La Sapienza, via Eudossiana 18, 00184 Rome, Italy

ARTICLE INFO

Article history:
Received 4 June 2009
Received in revised form
11 November 2009
Accepted 16 November 2009
Handling Editor: M.P. Cartmell
Available online 31 December 2009

ABSTRACT

This work deals with a study of the vibrational properties of carbon nanotube-reinforced composites by employing an equivalent continuum model based on the Eshelby–Mori–Tanaka approach. The theory allows the calculation of the effective constitutive law of the elastic isotropic medium (matrix) with dispersed elastic inhomogeneities (carbon nanotubes). The devised computational approach is shown to yield predictions in good agreement with the experimentally obtained elastic moduli of composites reinforced with uniformly aligned single-walled carbon nanotubes (CNTs). The primary contribution of the present work deals with the global elastic modal properties of nano-structured composite plates. The investigated composite plates are made of a purely isotropic elastic hosting matrix of three different types (epoxy, rubber, and concrete) with embedded single-walled CNTs. The computations are carried out via a finite element (FE) discretization of the composite plates. The effects of the CNT alignment and volume fraction are studied in depth to assess how the modal properties are influenced both globally and locally. As a major outcome, the lowest natural frequencies of CNT-reinforced rubber composites are shown to increase up to 500 percent.

1. Introduction

In the past decade, nano-structured materials have gained significant importance from a technological point of view for the wide range of engineering applications that require high levels of structural performance and multi-functionality. Interest has been growing continuously towards carbon nanotubes (CNTs) which, by virtue of their mechanical, thermal and electrical properties, have the potential to become the building blocks of a new generation of composite materials. The hosting matrix of the composite materials can comprise elastomeric materials or resins (e.g., epoxy), or cementitious materials as for high-performance fibre-reinforced cementitious composites. In [1] the addition of 1 phr (part per hundred parts of resin) of multi-walled carbon nanotubes (MWCNTs) in a styrene-butadiene copolymer resulted into a 45 percent increase in the elastic modulus and a 70 percent increase in the tensile strength. All the gathered experimental data further showed that the orientation of the nanotubes plays a major role in the mechanical reinforcement.

Here, the primary focus is on the free vibrational properties of these materials which allow to predict and interpret both the equilibrium and dynamic response, also in the nonlinear regime.

It has been widely recognised that different methodologies must be concurrently integrated to model properly complex nano-structured materials. This idea has mostly led to multi-scale approaches whereby a hierarchical combination of

* Corresponding author: Tel.: +39 6 44585 293; fax: +39 6 4884852.
E-mail address: walter.lacarbonara@uniroma1.it (W. Lacarbonara).

0022-460X/$ - see front matter © 2009 Elsevier Ltd. All rights reserved.
doi:10.1016/j.jsv.2009.11.020

continuum mechanics and molecular dynamics simulations is exploited to investigate the interplay between the macroscopic elastic features and the nano-structure. At the nano-structural level, the carbon nanotube constituents and their interactions with the matrix are described by introducing the proper constitutive equations at the molecular level. Most of the equivalent continuum approaches rely on the results of the Eshelby theory [2,3] complemented by several attempts of generalisation to heterogeneous bodies. In all of these theories, the interface between the hosting material and the embedded inhomogeneities (fibres, particles, carbon nanotubes, voids, and so on) plays a crucial role both on physical and mathematical grounds [4,5].

The major step towards modelling materials with fully dispersed inhomogeneities was undertaken by Mori and Tanaka [6]. In particular, they accounted for the presence of multiple inclusions and boundary conditions and their interactions. In [7] the homogenisation procedure, based on the Eshelby theory, under small deformations and small volume fractions of the embedded phases, has been used to determine the bulk and shear moduli and Landau coefficients of the composite material. Previous studies had established the validity of the Eshelby–Mori–Tanaka approach in determining the effective properties of composites reinforced with short, misaligned, carbon fibres, and with carbon nanotubes [8–11]. In [12] an approximate closed-form micro-mechanics model was proposed for estimating the effective elastic modulus. The model accounted for the nanotube curvature and length, and random dispersions of the nanotubes.

A few studies have addressed some aspects of the vibratory behaviour of CNTs and their composites. Among these aspects, it is worth mentioning modelling and simulation of vibrating nanotubes, studies of nano-mechanical resonators and oscillators, the use of vibration measurements to characterise the nanotube mechanical properties, the nanotube-induced enhancement of dynamic structural properties of composites, vibrations of nanotube-based sensors and actuators [13].

In particular, the enhanced damping properties of CNT-reinforced polymer composites have attracted a great deal of attention. The interfaces between nanotubes and polymer matrix, that turn out to be order of magnitude greater than those of traditional composites, may exhibit interfacial slippage that can cause high mechanical damping [14]. In [15], free and forced vibration tests were conducted on samples. They observed that the enhancement in damping ratio (up to 700 percent increase for MWCNT-epoxy beam as compared to the plain epoxy beam) is more important than enhancement in stiffness. Multi-walled nanotubes were observed to be a better reinforcement than single-walled nanotubes (SWCNTs). Similar results were obtained in [16], where the enhanced performance in terms of Young's modulus and wave propagation velocity has been numerically tested on the basis of an equivalent Euler–Bernoulli beam model derived from the Eshelby–Mori–Tanaka homogenisation procedure.

In this work, we present a theoretical and computational model for the elastodynamic response of CNT-reinforced composites that is employed to investigate the elastic properties of the resulting nano-structured materials when the hosting matrix is made of epoxy, rubber or concrete. By FE discretization of the constructed equivalent continuum model, we carry out a study of the vibrational properties of the composite plates, both from a global and a local point of view. In a global sense, we characterise the dependence of the frequencies on the volume fraction and on the alignment of the CNTs. From a local standpoint, we study the localisation patterns of the modal energy in terms of the distortional part of the elastic modal energy associated with the von Mises stresses. This study aims to highlight the way the energy may be optimally dissipated in the different vibration modes. At the same time, possible failure mechanisms under sustained vibrations are outlined as a by-product of the study.

The paper is organised as follows. In Section 2, we present the equivalent continuum model; in Section 3, extensive comparisons of the equivalent continuum model with the full three-dimensional theory are carried out for a reference volume element; in Section 4, the effective Young moduli are compared with existing experimental results. Section 5 summarises the studies about the dependence of the elastic properties of the composites on the alignment of the CNTs. Section 6 presents the most significant aspects of the modal properties of cantilevered CNT-reinforced plates made of epoxy, rubber, and concrete. In Section 7, the conclusions are drawn.

2. Equivalent continuum model

The equivalent continuum model is based on a low volume-fraction of cylindrical inhomogeneities, representative of the CNTs, embedded into a linearly elastic isotropic matrix.

There are different approaches to devising such a model, as shown in several works dealing with the general problem of equivalent continuum characterisation of composite materials where the inhomogeneities can be fibres or particles or defects [4]. Broadly speaking, there are two leading approaches. One approach formulates the configurational forces acting at the interface between the two materials. The second approach, widely used in computational schemes, carries out directly a characterisation of the continuum (macroscopic) elastic response on the basis of suitably assumed stress and deformation patterns [4,10].

The nano-structured composite material is made of two domains, $\mathcal{B}_M$ (hosting matrix) and $\mathcal{B}_C$ (CNTs) such that $\mathcal{B}=\mathcal{B}_M\cup\mathcal{B}_C$ is the reference configuration of the composite material. A representative quantity of the relative sizes of the two domains is the volume fraction $n_C=V_C/V$, where V_C is the volume of CNTs, and V is the volume of the overall composite material. Thus the volume fraction of the hosting matrix is $n_M=1-n_C$.

The proposed model is framed within the Eshelby theory for elastic inclusions. The original theory of Eshelby [2,3] is restricted to one single inclusion in a semi-infinite elastic, homogeneous and isotropic medium. The theory, generalised by Mori and Tanaka [6], allows to extend the original approach to the practical case of multiple inhomogeneities embedded into a finite domain [17]. In both cases there is an apparently similar but different definition of the Eshelby tensor, which depends on how the stress distribution, caused by the eigenstrain due to the inclusion, is described in the hosting matrix (see [18,19] for more details). When the equivalent elastic properties are considered to be independent on such an eigenstrain field, the simplest way to account for the presence of the inhomogeneities is to consider averaged strains and stresses.

Within this framework, let the elastic tensor for the matrix be $\mathbf{L}_M$ and that for the CNTs be $\mathbf{L}_C$. The constructed theory leads to a macroscopic equivalent elastic constitutive equation for the composite material in the form

$$\mathbf{T}(\boldsymbol{x}) = \hat{\mathbf{T}}(\mathbf{E}) = \mathbf{L} : \mathbf{E}(\boldsymbol{x}), \quad \boldsymbol{x} \in \mathcal{B} \tag{1}$$

where the stress tensor $\mathbf{T}$ and the infinitesimal strain tensor $\mathbf{E}$ are the tensor-valued quantities describing the equivalent elastic continuum at position $\boldsymbol{x} \in \mathcal{B}$. The Gibbs notation is adopted; $(:)$ indicates the inner product between tensors, and $(\cdot)$ here and henceforth denotes the dot product.

Various sophisticated methods can be devised by tuning differently the influence of the material phases through the volume fraction (for a deeper insight see [20]). The Eshelby–Mori–Tanaka approach, based on the equivalent elastic inclusion idea of Eshelby and the concept of *average stress* in the matrix due to Mori and Tanaka, is also known as the *equivalent inclusion-average stress* method. According to Benveniste's revisitation [10], the following expression of the effective elastic tensor is obtained:

$$\mathbf{L} = \mathbf{L}_M + n_C \langle (\mathbf{L}_C - \mathbf{L}_M) \cdot \mathbf{A} \rangle \cdot [n_M \mathbf{I} + n_c \langle \mathbf{A} \rangle]^{-1} \tag{2a}$$

$$\mathbf{A} = [\mathbf{I} + \mathbf{S} \cdot \mathbf{L}_M^{-1} \cdot (\mathbf{L}_C - \mathbf{L}_M)]^{-1} \tag{2b}$$

where $\mathbf{I}$ represents the fourth-order unit tensor; $\mathbf{S}$ is the fourth-order Eshelby tensor that is specialised to the case of cylindrical inclusions representative of the CNTs and depends on their orientation; $\mathbf{A}$ is a fourth-order tensor referred to as *concentration factor*; the brackets denote an average over all possible orientations of the inclusions.

In the computational implementation, the orientation of the CNTs is accounted for by rotating the elastic tensor of the inclusions. This is achieved by introducing a suitable rotation tensor that acts on the Eshelby tensor $\mathbf{S}$ and then on the equivalent elastic tensor $\mathbf{L}$ [21]. In particular, one can prove that rotating $\mathbf{S}$ results into the rotation of $\mathbf{A}$. To parametrise correctly the rotations, we considered two Euler angles only, (ϕ, ψ), excluding the immaterial spin rotation of the CNTs around their axes. The simplest configuration for the nano-structured material is obtained when the nanotubes are collinear with a unit vector, whence the material behaviour becomes transversely isotropic. In this case, the rotation tensor is uniform throughout the domain: $\langle \mathbf{A} \rangle = \mathbf{A}$ and $\langle (\mathbf{L}_C - \mathbf{L}_M) \cdot \mathbf{A} \rangle = (\mathbf{L}_C - \mathbf{L}_M) \cdot \mathbf{A}$. The ensuing equivalent elastic tensor is uniform and is given by the expression

$$\mathbf{L} = \mathbf{L}_M + n_C (\mathbf{L}_C - \mathbf{L}_M) \cdot \mathbf{A} \cdot [n_M \mathbf{I} + n_c \mathbf{A}]^{-1} \tag{3}$$

On the contrary, when the nanotubes are randomly oriented in space, suitable statistical distribution functions must be used in the averaging process over the ranges of variation of the Euler angles.

3. Comparison of the equivalent continuum model with the full three-dimensional theory

The reliability of the equivalent continuum model is assessed considering a description of the elastic interactions between the CNTs and the elastic matrix within the context of the full three-dimensional theory. To this end, some paradigmatic loading conditions are imposed on a reference cylindrical cell made of two coaxial cylinders: an individual CNT-SWNT(10,10) embedded into a cylindrical matrix of epoxy resin, as shown in Fig. 1. The mechanical parameters of the two materials, taken from those available in the literature, and the cell geometric characteristics are reported in Table 1. The computed stresses are normalised with respect to the Lamé constant of the epoxy resin, $\lambda = 4.7\,\text{GPa}$; the lengths and displacements are normalised with respect to the value of 8.5 nm, nearly 10 times the CNT radius, which can be considered a sufficiently low value of CNT aspect ratio (i.e., the ratio between the CNT length and its diameter). In fact, some preliminary numerical investigations showed that the enhanced properties of the composite material at the scale of such a specimen cannot be appreciated as the aspect ratio increases towards the upper bound (i.e., $10^2 - 10^3$). Furthermore, the performance of the homogenised continuum model can be investigated more effectively considering low aspect ratios, for which the different properties of the equivalent continuum model are better emphasised with respect to the three-dimensional elasticity treatment of the two materials.

Note that the FE analyses are performed assuming a compatible continuity in the displacement field across the surface interface between the matrix and nanotubes. This is a plausible assumption since we are interested in the linear elastic response away from de-bonding phenomena.

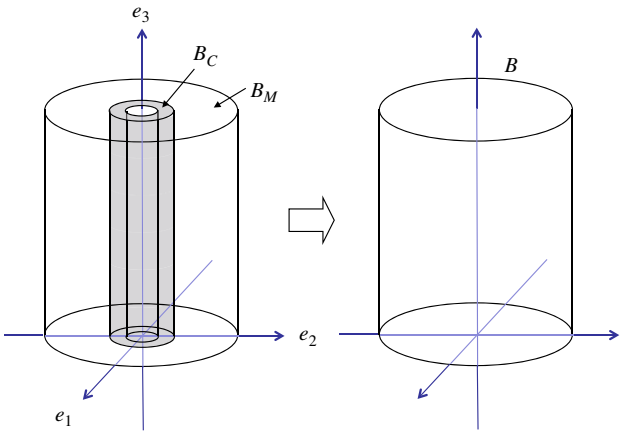

Fig. 1. The reference cell.

Table 1
Reference cell characteristics.

	Epoxy resin	SWNT(10,10)
E (Young's modulus) (GPa)	3.3	970
v (Poisson's ratio)	0.4	0.28
G (shear modulus) (GPa)	1.18	450
(Average radius) (nm)	4.675	0.4675
(Thickness) (nm)	7.65	0.765
(Height) (nm)	34	34

By employing Voigt's notation, the stress and strain tensors are described by the following six-dimensional algebraic vectors:

$$\mathbf{T}^{\top} = [T_{11}\ \ T_{22}\ \ T_{33}\ \ T_{23}\ \ T_{13}\ \ T_{12}]\ ,$$
$$\mathbf{E}^{\top} = [E_{11}\ \ E_{22}\ \ E_{33}\ \ E_{23}\ \ E_{13}\ \ E_{12}] \tag{4}$$

The compliance tensor $\mathbf{M}$ $(=\mathbf{L}^{-1})$ takes the standard form of an orthotropic material which preserves symmetries with respect to an axis collinear with the nanotubes. Hence, the compliance elastic coefficients are $M_{kk} = 1/E_k$ $(k=1,2,3)$, $M_{jk} = -v_{jk}/E_k$ $(j \neq k = 1,2,3)$, $M_{44} = 1/G_{23}$, $M_{55} = 1/G_{13}$, $M_{66} = 1/G_{12}$. This is due to the fact that both the hosting matrix and the nanotubes are assumed to be isotropic materials; moreover, the nanotubes are cylindrical inclusions. In consonance with various works supported by micro-mechanical modelling and experimental observations, the independent elastic coefficients are usually well approximated by five equivalent independent elastic coefficients (see for instance [17,16,9]). Actually, the nature of the twisted array of a SWCNT as a helical array is not completely transversely isotropic. Therefore, to develop a more general framework, which may handle also random distributions, we chose to consider the more general case of six independent elastic coefficients for the inclusions. In particular, in the treated case of uniformly aligned CNTs, the plane of the resulting transverse isotropy is orthogonal to the CNT axis. Therefore, the generic form of the elastic compliance matrix is simplified into an orthotropic symmetric representation with respect to the CNT axis.

In the present benchmark case, the CNT axis is collinear with the $\boldsymbol{e}_3$- axis, hence $E_1 \equiv E_2$, $v_{23} \equiv v_{13}$ and $G_{13} \equiv G_{23}$. From Table 1 the elastic coefficients of the equivalent orthotropic continuum are listed below:

$$E_1 \equiv E_2 = 3.74\,\text{GPa}, \quad E_3 = 9.42\,\text{GPa}, \quad v_{13} \equiv v_{23} = 0.399, \quad v_{12} = 0.56$$

$$G_{13} \equiv G_{23} = 1.20\,\text{GPa}, \quad G_{12} \equiv \frac{E_1}{2(1+v_{12})} = 1.19\,\text{GPa}$$

The comparisons between the inhomogeneous cell (henceforth denoted *in-cell*) and the equivalent continuum cell (denoted *eq-cell*) are in terms of non-dimensional total stored energy (recall that the stresses have been taken in their ratios to $\lambda = 4.7$ GPa). The results are reported in Table 2.

We observe that the equivalent continuum model is capable of representing accurately uniform tests, without appreciable differences with respect to the reference model. Local effects arising in the boundary layers occur mainly in the torsional and shear displacement-driven tests. Obviously, such boundary layers can not be described by the equivalent

Table 2
Non-dimensional total stored energy: comparison between inhomogeneous cell (in-cell) and equivalent continuum cell (eq-cell).

Displacement driven	in-cell	eq-cell	Error (%)
Longitudinal	7.97×10^{-3}	7.98×10^{-3}	0.0
Radial (longitudinally constrained)	0.175	0.227	22.9
Radial (longitudinally free)	0.310	0.317	2.2
Torsional	5.0×10^{-4}	5.7×10^{-4}	12.3
Shear	8.52×10^{-4}	9.69×10^{-4}	12.1

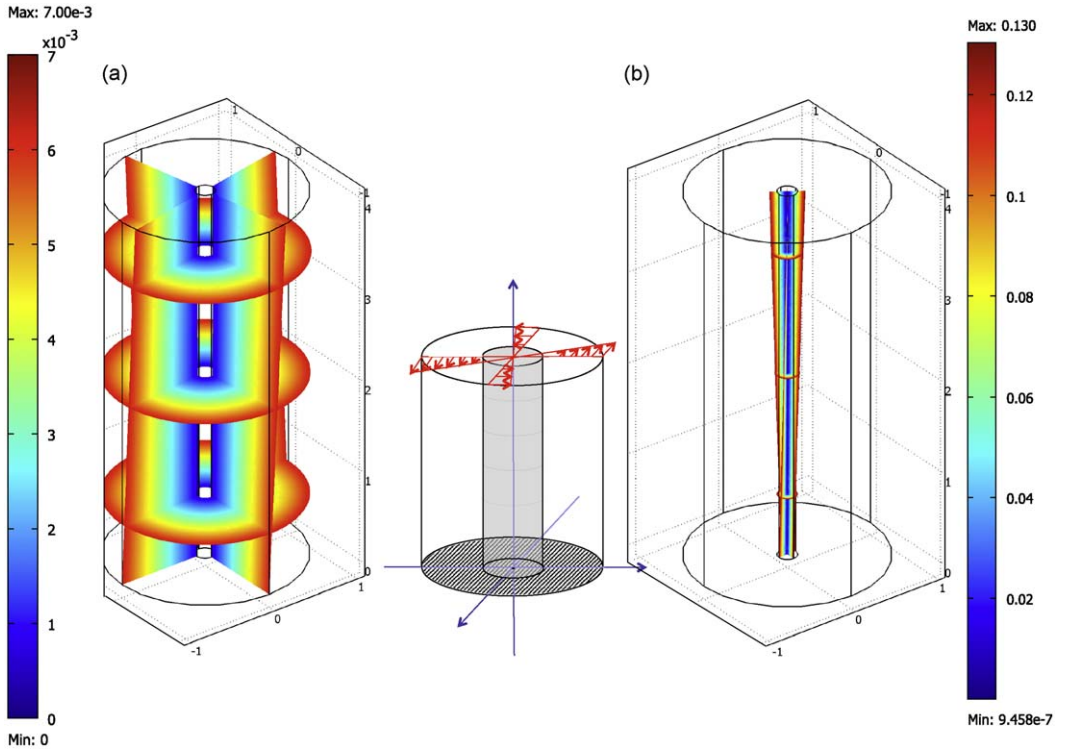

Fig. 2. Torsional test with the reference model: non-dimensional tangential stress distribution along the *z*-axis in (a) the hosting matrix and (b) in the CNT.

continuum model that yields recognisable bounded differences. This point is emphasised in Figs. 2 and 3. The same result is pointed out by the comparisons in the shear test of Fig. 4.

4. Comparison of the equivalent continuum results with existing experimental results

The approach illustrated in Section 2 has been employed to predict the effective elastic modulus of CNT-reinforced nano-composites for which experimental data are available. To make these comparisons meaningful, it is essential that the synthesis of the nano-composites is carried out with accurate control of the micro-structure of the composites. In particular, special attention has to be devoted to the following aspects: homogeneous dispersion, efficient interfacial stress transfer, and good alignment. One of the few works where these requirements seem to be well fulfilled is [22]. The SWNTs, produced by catalytic chemical vapour deposition, had diameters of about 1–2 nm and lengths of about 5–15 μm. We did not consider the case of functionalised SWNTs since the functionalisation typically alters the mechanical properties of the carbon nanotubes. On the contrary, we focused on pristine SWNTs, with a weight fraction equal to 0.5 percent, which were uniformly dispersed into epoxy and aligned by means of a reactive spinning process. The composites were characterised by optical and electron microscopy and tensile tests. The tensile tests delivered a Young modulus of 3.47 GPa.

To carry out the calculation of the effective elastic modulus within our theoretical framework, we had to compute the CNT volume fraction n_C, one of the input data. We assumed the specific weights of 1.20×10^3 kg/m^3 for the epoxy resin

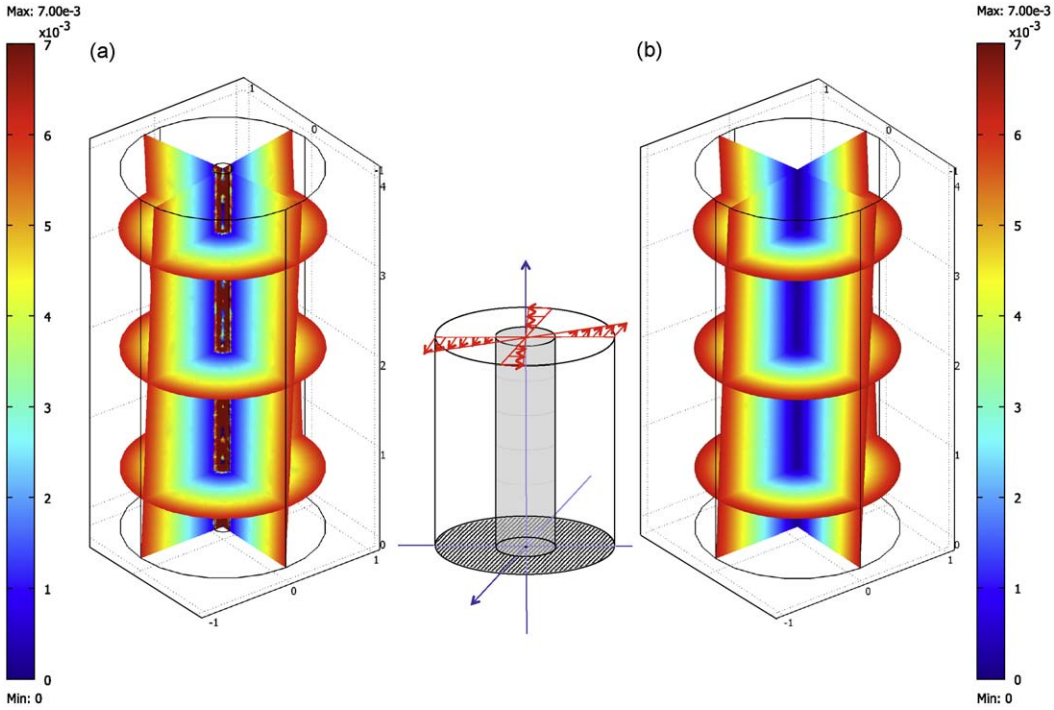

Fig. 3. Torsional test: comparison of non-dimensional tangential stress distributions (τ) along the z-axis obtained with (a) the reference model and (b) the equivalent model. For the sake of clarity, in plot (a) the actual range of $\tau \in [10^{-6}, 0.13]$ was restricted to $\tau \in [10^{-6}, 7 \times 10^{-3}]$.

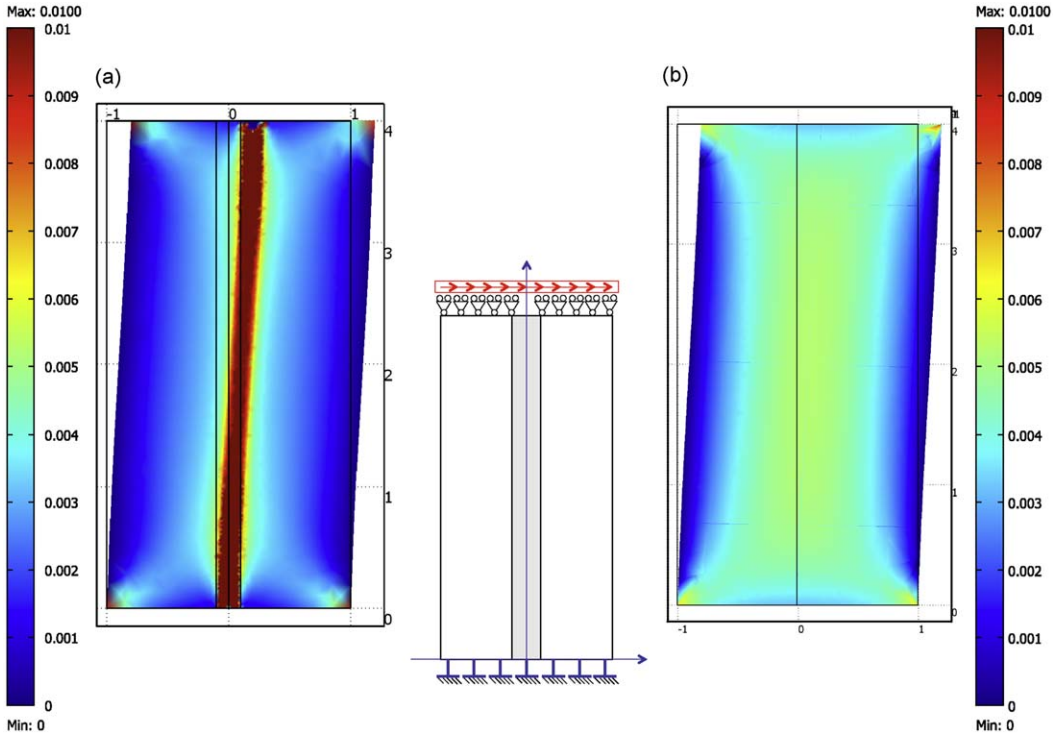

Fig. 4. Shear test: comparison of non-dimensional tangential stress distributions along the z-axis obtained with (a) the reference model and (b) the equivalent model. For the sake of clarity, in plot (a) the actual range of $\tau \in [-0.01, 0.07]$ was restricted to $\tau \in [0, 10^{-2}]$.

and $7.85/6 \times 10^3\,\mathrm{kg/m^3}$ for the CNTs, respectively. The resulting CNT volume fraction turns out to be $n_C = 0.46$ percent. In agreement with the experimentally measured characteristics, in the numerical computations we employed the following mechanical parameters: $(E, \nu, \lambda) = (2.35\,\mathrm{GPa},\ 0.4,\ 3.357\,\mathrm{GPa})$ for the epoxy resin and $(E, \nu) = (970\,\mathrm{GPa},\ 0.28)$ for

the CNTs, respectively. The thus calculated elastic modulus is 3.27 GPa which is only 5 percent lower than the experimentally measured value.

5. Influence of the carbon nanotube alignment on the effective elastic properties

In this section, we summarise the results of the studies about the influence of the CNT alignment on the elastic properties of the nano-structured composites. Fig. 5 shows the scheme of the performed computational tests in terms of geometry, constraints, and loading conditions. The reference body is a plate-like three-dimensional body, subject to a uniform uniaxial pressure on two opposite edges. The other two edges as well as the top and bottom surfaces are stress-free.

We evaluated the apparent stiffness coefficient expressed as

$$K_{11}(\phi) \coloneqq \frac{T_{11}(\phi)}{E_{11}} = L_{11}(\phi) + \frac{E_{22}}{E_{11}} L_{12}(\phi) + \frac{E_{33}}{E_{11}} L_{13}(\phi) + \frac{E_{12}}{E_{11}} L_{16}(\phi) \tag{5}$$

where ϕ denotes the angle between the CNT axis and the assumed loading direction $\boldsymbol{e}_1$. Fig. 6 shows the variation of $K_{11}(\phi,\boldsymbol{x})/K_{11}(0,\boldsymbol{x})$ with the angle ϕ. When $\phi = 0$ all CNTs are aligned transversally to the loading direction while $\phi = \pi/2$ represents the case of uniform alignment with the loading direction. The test was numerically conducted using the following mechanical parameters: $(E, v) = (970\,\text{GPa},\ 0.28)$ for the CNTs and $(E, v, \lambda) = (3.3\,\text{GPa}, 0.4, 4.7\,\text{GPa})$ for the epoxy resin, respectively. The results, normalised with respect to the epoxy's Lamé constant, show the predictable increase of stiffness as the CNTs tend to be aligned with the loading direction. However, this increase is not monotonic. When the CNTs are slightly rotated from the transverse direction by small angles ϕ, the coefficient K_{11} decreases mildly. This is due to the dependence of the apparent longitudinal elastic coefficient K_{11} on both the longitudinal and transverse elastic properties. K_{11} decreases up to about $\phi = \pi/8$; at the same time, the coefficient L_{12} decreases with a higher rate than the rate of increase of L_{11}. As shown in Fig. 7, the remarkable influence of such a type of Poisson's effect caused by the orientation of the transverse CNTs prevails over the longitudinal elastic properties.

6. Vibrations of carbon nanotube-reinforced composites

The free vibration properties of carbon nanotube-reinforced composites are investigated with a twofold objective: (i) to unfold the fundamental modal properties—that generally allow to study and interpret the equilibrium and dynamic response—and (ii) to determine the way the vibrational energy may be optimally dissipated in the vibration modes of the CNT-reinforced composite. Specific sets of experiments encouraged these investigations: in [14], to cite only one, it has been shown that, by embedding oxidised SWNTs into polycarbonate with 2 percent weight fraction, the loss modulus (hence, the damping coefficient) increased by more than an order of magnitude (>1000 percent) with respect to the baseline polycarbonate. However, this aspect will be the subject of a forthcoming paper.

First we investigated the effects of the CNTs volume fraction and alignment on the natural frequencies of three different hosting materials, namely, epoxy (Epx), rubber (Ru), and concrete (Be). These materials are massively used in various engineering fields. In particular, epoxy is used in the laminated composites of aeronautical structures, concrete is the most widely used material in the civil construction industry. Vulcanised rubber, due to its high elasticity and strength arising from the vulcanisation process, is used as baseline material in several industrial applications, especially as damping or vibration–isolation material or as sealing material.

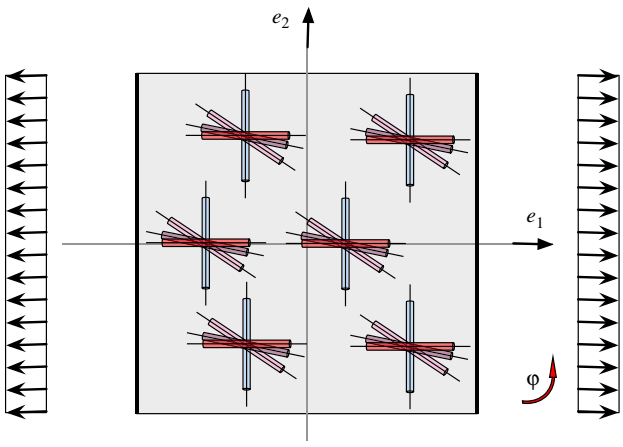

Fig. 5. Tensile test varying the CNT alignment.

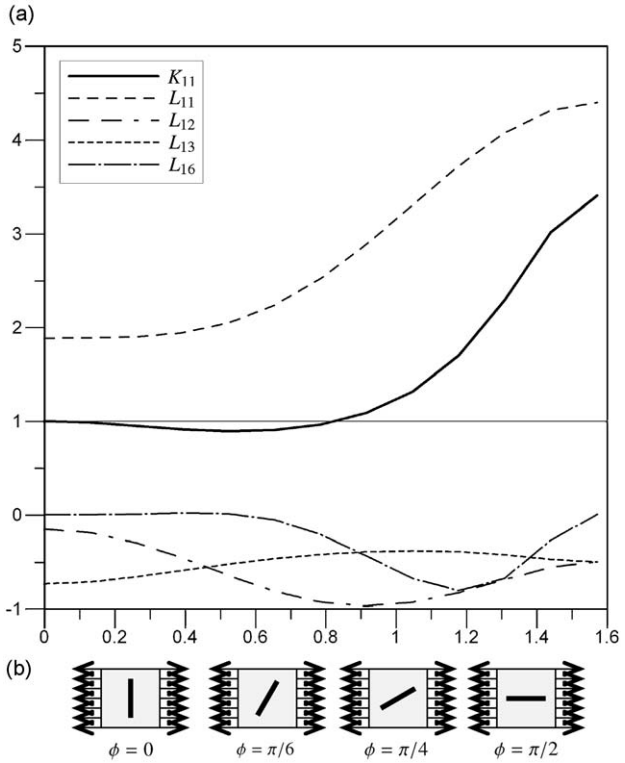

Fig. 6. Variation of the stiffness coefficients with the angle ϕ: the coefficients are normalised with respect to $K_{11}(0, \boldsymbol{x})$.

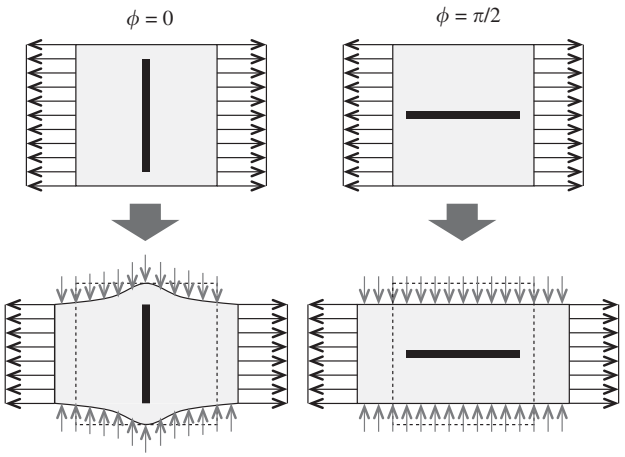

Fig. 7. Effect of increasing K_{11} due to the lateral constrained contraction caused by the CNTs.

It is worth mentioning that some previous theoretical works investigated also the influence of the CNT aspect ratio on the composite mechanical properties (see for instance [8]). However, we did not account for the CNT aspect ratio, relying on the numerical results that showed the substantial independence of the effective Young modulus on the aspect ratio when the latter ranges from 50 to 1000 [16].

The equations of motion for the free vibration problem, used in the employed (PDE-mode) FE discretization, are

$$\boldsymbol{\nabla} \cdot \mathbf{T}^{\top} = \rho \ddot{\boldsymbol{u}}, \quad \forall \boldsymbol{x} \in \mathcal{B}, \ \ t \in (0, \infty) \tag{6}$$

where $\boldsymbol{\nabla} = \boldsymbol{e}_1 \partial/\partial x_1 + \boldsymbol{e}_2 \partial/\partial x_2 + \boldsymbol{e}_3 \partial/\partial x_3$ is the del vector, here expressed in the orthonormal basis $\{\boldsymbol{e}_1, \boldsymbol{e}_2, \boldsymbol{e}_3\}$, the overdot indicates differentiation with respect to time, $\boldsymbol{u}$ is the displacement field, ρ is the equivalent mass per unit volume of the reference configuration. The effect on the mass density of small volume fractions of carbon nanotubes is neglected. The constitutive equation of the equivalent continuum is given by Eq. (1) where $\mathbf{L}$ is expressed by Eq. (2a). We substitute

the strain–displacement relationships $\mathbf{E}=[(\nabla \boldsymbol{u})^{\top}+\nabla \boldsymbol{u}]/2$ into (1) and the resulting stress, $\mathbf{T}=\mathbf{L}:[(\nabla \boldsymbol{u})^{\top}+\nabla \boldsymbol{u}]/2$, into the balance equations given by (6). The boundary conditions are $\mathbf{T}=\mathbf{0}$ on the bottom and upper surfaces and on the two free lateral surfaces. On one of the two edges, the displacement is inhibited in all directions, thus $\boldsymbol{u}=\mathbf{0}$.

The problem is suitably non-dimensionalised introducing a characteristic length (corresponding to the length of the specimen) and a characteristic circular frequency $\omega_c=\sqrt{E_{11}/(\rho a^2)}$ where a is a characteristic length, equal to the square of the longitudinal length divided by the radius of inertia of the plate cross section of unitary width, and E_{11} is the longitudinal modulus of the hosting matrix in the $\boldsymbol{e}_1$–direction. This means that the characteristic stress with which the stresses are rendered non-dimensional is the elastic modulus E_{11}.

6.1. Variation of the frequencies

An eigenvalue analysis was conducted varying the CNTs alignment in the specimen of Fig. 5, where we removed the tensile loads, and clamped the left edge. The mechanical properties of the composite plates are those employed in the tests of Section 5. The frequencies of the lowest 10 modes of the specimen, made of the pure matrix only and of the composite CNT-reinforced material, are compared in Table 3. We considered the ratios of the frequencies to the lowest frequency of the equivalent homogeneous, isotropic, all-matrix, cantilevered plate. When we take the specimen made only of the matrix material, this ratio becomes 1 in the first mode. Moreover, we normalised the mode shapes according to $\int_B \boldsymbol{\phi}_k\cdot\boldsymbol{\phi}_k\,\mathrm{d}V=1,\ \forall k=1,2,\ldots$, where $\boldsymbol{\phi}_k(\boldsymbol{x})$ denotes the kth mode shape of the plate.

The comparison in terms of the frequencies for the case of epoxy clearly emphasises the fact that the nano-structured composite material exhibits improved mechanical properties. In particular, for the specific conducted tests, the lowest frequency of the specimen with longitudinally oriented CNTs ($\phi=\pi/2$) is about 100 percent that of the specimen with the homogeneous matrix material.

We thus studied the influence of the CNTs volume fraction on the frequencies and mode shapes in the case of optimal CNT alignment, $\phi=\pi/2$ (see Table 4). The CNTs alignment, which is optimised for the considered specimen, results into

Table 3
Variation of the frequencies of the lowest 10 vibration modes with the CNTs orientation when $n_C=1\%$.

Mode	1	2	3	4	5	6	7	8	9	10
Matrix	1.07	2.41	6.16	6.45	7.92	8.63	14.66	15.73	17.18	17.19
$\phi=0$	0.30%	1.27%	3.32%	1.50%	11.08%	48.76%	9.66%	8.81%	1.57%	7.18%
$\phi=\pi/12$	2.12%	4.83%	3.86%	6.06%	12.03%	44.13%	9.23%	8.67%	6.46%	12.83%
$\phi=\pi/6$	10.74%	11.17%	6.43%	17.50%	10.74%	36.22%	10.38%	3.68%	8.33%	14.61%
$\phi=\pi/4$	32.97%	16.36%	14.52%	28.51%	7.98%	36.11%	5.92%	14.17%	14.27%	18.51%
$\phi=\pi/3$	60.06%	22.87%	27.22%	27.46%	11.89%	42.94%	8.21%	26.42%	23.09%	31.08%
$\phi=5\pi/12$	81.83%	26.14%	28.54%	25.72%	31.51%	45.55%	14.55%	20.77%	36.60%	59.14%
$\phi=\pi/2$	92.03%	25.88%	27.19%	25.80%	44.31%	43.54%	18.28%	17.00%	37.98%	52.99%

The variations are given in % increments with respect to the frequencies of the all-matrix material.

Table 4
Variations of the frequencies of the lowest 10 vibration modes with the volume fraction when $\phi=\pi/2$.

Mode	1	2	3	4	5	6	7	8	9	10
Matrix	1.07	2.41	6.16	6.45	7.92	8.63	14.66	15.73	17.18	17.19
$n_C=0.25\%$	28.04%	6.77%	17.34%	12.26%	6.79%	12.29%	3.46%	13.49%	15.15%	18.69%
$n_C=0.5\%$	52.03%	13.40%	22.68%	18.57%	19.78%	23.71%	8.15%	14.19%	25.58%	34.59%
$n_C=1.0\%$	92.03%	25.88%	27.19%	25.80%	44.31%	43.54%	18.28%	17.00%	37.98%	52.99%
$n_C=2.0\%$	150.90%	44.63%	31.06%	32.80%	75.26%	67.59%	27.49%	21.40%	48.78%	61.98%
$n_C=5.0\%$	265.81%	85.15%	39.37%	42.90%	119.72%	104.71%	35.27%	41.73%	61.41%	79.49%
$n_C=10.0\%$	385.94%	131.64%	50.96%	54.42%	142.36%	143.06%	51.55%	62.81%	74.56%	100.41%

The variations are given in % increments with respect to the frequencies of the all-matrix material.

Table 5
Mechanical parameters of the different hosting matrix materials.

	Rubber	Concrete	CNT
Young's modulus (GPa)	0.1	30	970
Poisson's ratio	0.48	0.2	0.28
Lamé's constants (GPa)	0.81	8.34	

significant frequency increases for those modes whose associated modal stiffness is substantially affected by the alignment, namely the first, second, fifth, and sixth modes. In particular, the frequency of the lowest mode increases by nearly 400 percent when the volume fraction is increased from 0.25 to 10 percent. On the contrary, when the alignment

Table 6
Variations of the frequencies of the lowest 10 vibration modes with the CNTs orientation for CNT-reinforced rubber (Ru).

Mode Ru	1 1.1	2 2.37	3 6.17	4 6.29	5 8.04	6 8.61	7 14.64	8 15.53	9 16.65	10 17.50
$\phi=0$	4.98%	2.45%	8.24%	9.39%	13.07%	105.37%	22.23%	16.29%	21.01%	68.81%
$\phi=\pi/12$	5.00%	17.92%	12.02%	15.58%	24.15%	96.97%	23.82%	31.99%	24.21%	63.64%
$\phi=\pi/6$	20.96%	61.16%	18.73%	31.58%	42.19%	89.09%	19.13%	37.38%	41.27%	51.24%
$\phi=\pi/4$	69.80%	136.64%	38.85%	49.03%	53.21%	103.39%	20.24%	41.51%	53.66%	54.54%
$\phi=\pi/3$	157.06%	186.09%	50.23%	84.66%	49.01%	123.07%	48.68%	41.14%	52.24%	64.97%
$\phi=5\pi/12$	309.86%	202.10%	44.46%	75.25%	109.50%	135.02%	50.89%	59.99%	55.86%	74.09%
$\phi=\pi/2$	508.52%	187.85%	41.69%	58.63%	147.94%	155.74%	51.97%	54.48%	57.88%	73.75%

Table 7
Variations of the frequencies of the lowest 10 vibration modes with the CNTs orientation for CNT-reinforced concrete (Be).

Mode Be	1 1.01	2 2.48	3 6.03	4 6.59	5 7.58	6 8.63	7 14.58	8 15.54	9 16.17	10 17.79
$\phi=0$	0.77%	0.98%	1.07%	0.96%	9.71%	1.02%	3.25%	0.99%	0.82%	0.93%
$\phi=\pi/12$	0.81%	2.18%	0.98%	1.65%	8.42%	2.34%	3.67%	0.85%	0.91%	1.79%
$\phi=\pi/6$	1.52%	4.76%	1.33%	3.43%	6.23%	4.51%	4.52%	1.10%	1.65%	2.77%
$\phi=\pi/4$	3.93%	6.57%	3.33%	5.45%	4.33%	6.04%	5.09%	2.98%	3.73%	0.72%
$\phi=\pi/3$	8.33%	7.16%	8.15%	6.94%	3.83%	8.14%	6.53%	6.98%	9.22%	0.51%
$\phi=5\pi/12$	12.33%	4.94%	11.08%	7.59%	2.15%	6.86%	3.68%	11.85%	8.21%	0.46%
$\phi=\pi/2$	14.19%	4.13%	12.74%	7.82%	1.84%	6.92%	3.13%	12.48%	9.98%	1.78%

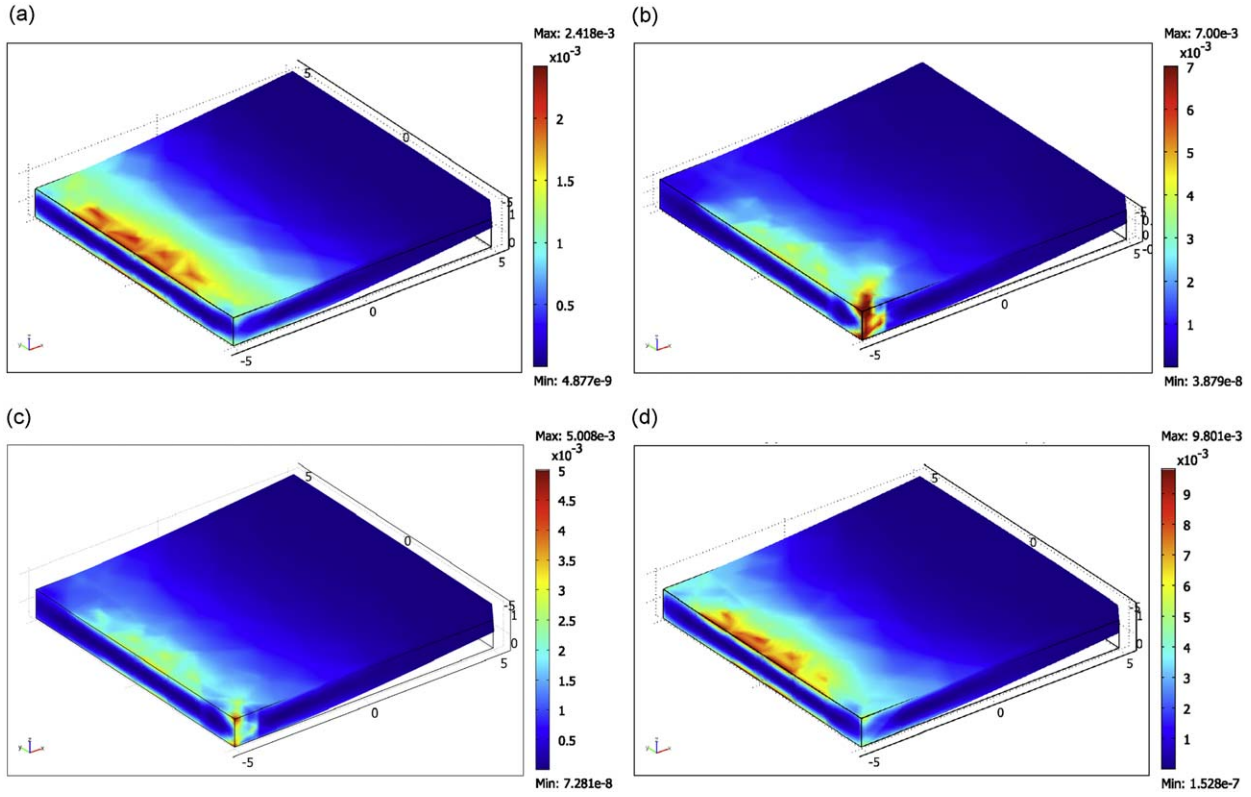

Fig. 8. Slices of the contour plots of the stored-energy function associated with the lowest mode: (a) pure matrix, aligned CNTs with (b) $\phi=\pi/4$, (c) $\phi=\pi/6$, and (d) $\phi=\pi/2$.

does not influence significantly the mode shapes, the frequency variations are less appreciable. This is the case with the third, fourth, seventh, and eighth modes. A CNT volume fraction of 10 percent leads, for these modes, to a frequency increment of the order of 50 percent.

However, it is worth mentioning that previous experimental tests showed that high concentrations of CNTs do not lead necessarily to improved mechanical properties. This is due to a complex phenomenon of CNTs agglomeration by which micro-voids can be formed in the material, thus making the mechanical response weaker. SEM images of the CNT composite with 4 percent weight fraction, reported in [23], furnish a good evidence of the mentioned phenomenon. These situations cannot be captured by an equivalent continuum model which, by imposing a homogenisation procedure, can describe only nano-structured materials with uniformly dispersed inclusions.

Thus we preferred to carry out similar investigations with different hosting materials, namely, silicone rubber and concrete, keeping the CNT volume fraction to a reasonable value, namely, 1 percent. The adopted mechanical parameters are given in Table 5. In the computations, such parameters are normalised with respect to the corresponding Lamé constant of the hosting matrix materials.

The variations of the frequencies of the lowest 10 vibration modes with the orientation angle, for rubber and concrete, respectively, are summarized in Tables 6 and 7, respectively. While we observe a remarkable increase of about 500 percent in the fundamental frequency of the CNT-reinforced rubber when the CNTs are longitudinally aligned, in the case of concrete the increase is about 10 percent. This is not surprising since the ratio between the elastic modulus of CNTs and that of rubber is of the order of 10^4 whereas this ratio is of the order of 30 for concrete. Thus the functionalisation of soft polymeric materials with perfectly aligned CNTs has the potential of changing substantially their mechanical properties.

6.2. Stored energy patterns of the vibration modes

The study of the fundamental properties of the vibration modes of nano-structured composites requires a more in-depth analysis of the spatial patterns of the stored-energy distributions in each individual mode. In particular, the spatial distribution of the *distortional* part of the stored energy allows to gain insight into potential failure mechanisms under sustained vibrations as well as into the dissipation properties of each mode.

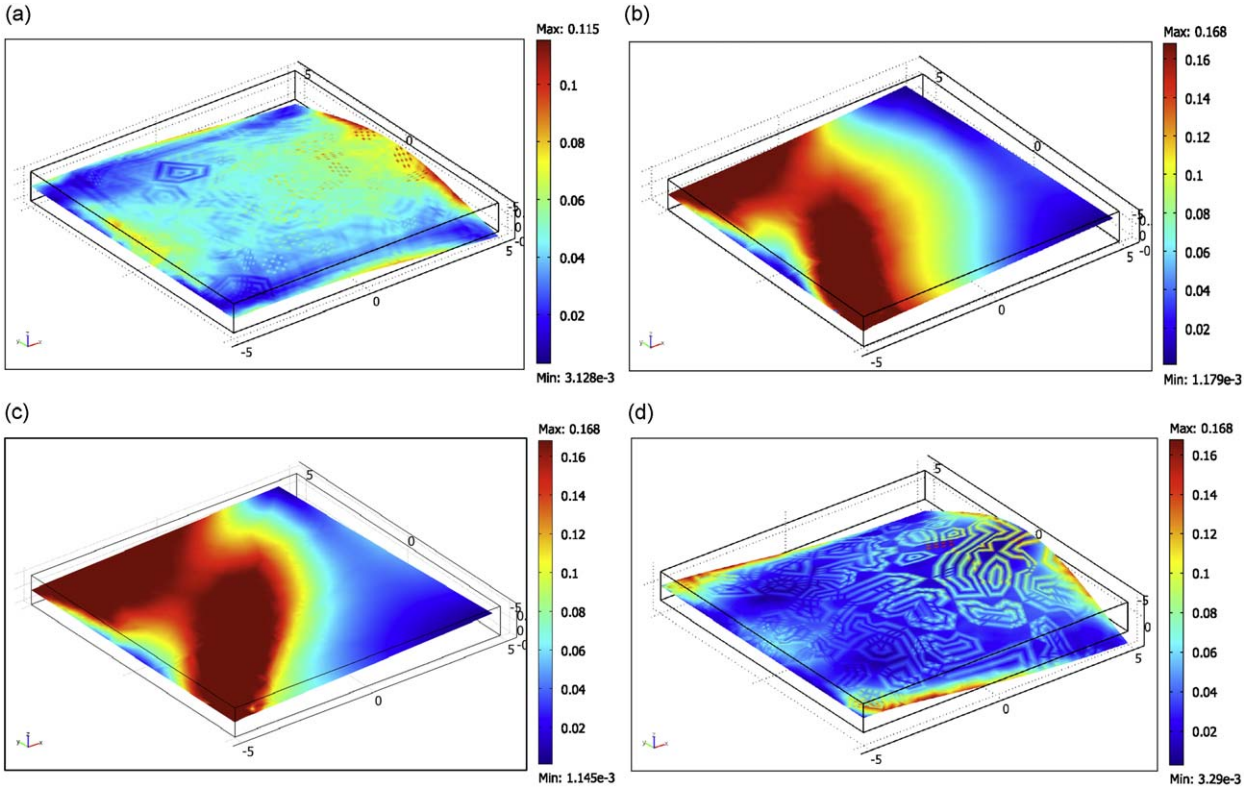

Fig. 9. Slices of the contour plots of the von Mises stress associated with modes possessing close frequencies in an epoxy-based (Epx) composite plate: (a) 5th mode of the all-matrix plate, (b) 4th mode of the CNT-reinforced (nano-composite) plate with $\phi = \pi/6$, (c) 4th mode of CNT-reinforced with $\phi = \pi/4$, and (d) 3rd mode of the nano-composite plate with $\phi = \pi/2$. For the sake of clarity, the ranges in plots (b) and (c) were bounded with respect to the actual ranges of [1e^{-3}, 1.153] and [5.5e^{-4}, 0.5], respectively.

It is known that the distortional stored energy is an effective tool for characterising the onset of yielding in ductile linearly isotropic bodies; in this case, the distortional stored-energy function is a pure-shear stored energy which can be written as $V^D = 3(\tau^O)^2/4G$, where G is the shear modulus and τ^O the *von Mises stress* (or *octahedral shear stress*). For a general anisotropic material, the specific stored-energy function can be decomposed into a direct summation of two contributions according to

$$V = \tfrac{1}{2} T^V \varepsilon^V + \tfrac{1}{2}\mathbf{T}^D : \mathbf{E}^D \tag{7}$$

where $T^V := (\mathrm{tr}\,\mathbf{T})/3$ indicates the magnitude of the spherical part of the stress tensor $\mathbf{T}^V = T^V\mathbf{I}$; $\mathbf{I} = \delta_{ij}\boldsymbol{e}_i\boldsymbol{e}_j$ represents the second-order identity tensor, $\varepsilon^V := \mathrm{tr}\,\mathbf{E} = 3E^V$ denotes the volumetric (or dilatational) strain, $\mathbf{E}^V = E^V\mathbf{I}$ is the spherical part of the strain tensor, while the superscript D indicates the deviatoric part of the corresponding tensors. For isotropic materials, there is a full elastic uncoupling between the spherical and deviatoric strain and stress components highlighted by the constitutive equations in their uncoupled form: $T^V = 3(\lambda + 2/3\mu)E^V$ and $\mathbf{T}^D = 2\mu\mathbf{E}^D$. Thus, in isotropic materials, there is a direct decomposition into a purely dilatational energy and a purely distortional energy. According to [24], the distortional energy interpretation for the von Mises yield criterion can be effectively used to construct yield criteria for particle-reinforced composites that bear isotropy properties. They indeed proposed a criterion that describes well the initial yield of particle-reinforced composites.

The situation is more complex with anisotropic materials for which, as known, there is no elastic uncoupling between spherical and deviatoric strain and stress components. Let us substitute the spherical part of the strain tensor, $\mathbf{E}^V := (\mathrm{tr}\,\mathbf{E})/3\mathbf{I}$, into constitutive Eq. (1), $\mathbf{T}^{(V)} = \mathbf{L} : \mathbf{E}^V$. The ensuing stress tensor $\mathbf{T}^{(V)} = \mathbf{L} : \mathbf{E}^V = E^V\mathbf{L} : \mathbf{I} = E^V L_{ijmm}\boldsymbol{e}_i\boldsymbol{e}_j \neq T^V\mathbf{I}$ is not spherical. This means that a purely dilatational/volumetric state of deformation does not induce a purely spherical state of stress in an anisotropic material and the energy calculated through $\frac{1}{2}T^V\varepsilon^V$ does not represent a purely dilatational stored energy. The same applies to the deviatoric part of the stored energy, $\frac{1}{2}\mathbf{T}^D : \mathbf{E}^D$. However, we can legitimately refer to these energies as *quasi-dilatational* and *quasi-distortional* stored energies. More generally speaking, the particular class of materials represented by our equivalent orthotropic continuum does not exhibit a decomposition into spherical and deviatoric parts in the constitutive equations. The calculated spherical part of the strain tensor

$$\mathrm{tr}\mathbf{E} \equiv \left(\frac{1}{E_1} - \frac{\nu_{12}}{E_2} - \frac{\nu_{13}}{E_3}\right)T_{11} + \left(\frac{1-\nu_{12}}{E_2} - \frac{\nu_{23}}{E_3}\right)T_{22} + \frac{1-\nu_{13}-\nu_{23}}{E_3}T_{33} \tag{8}$$

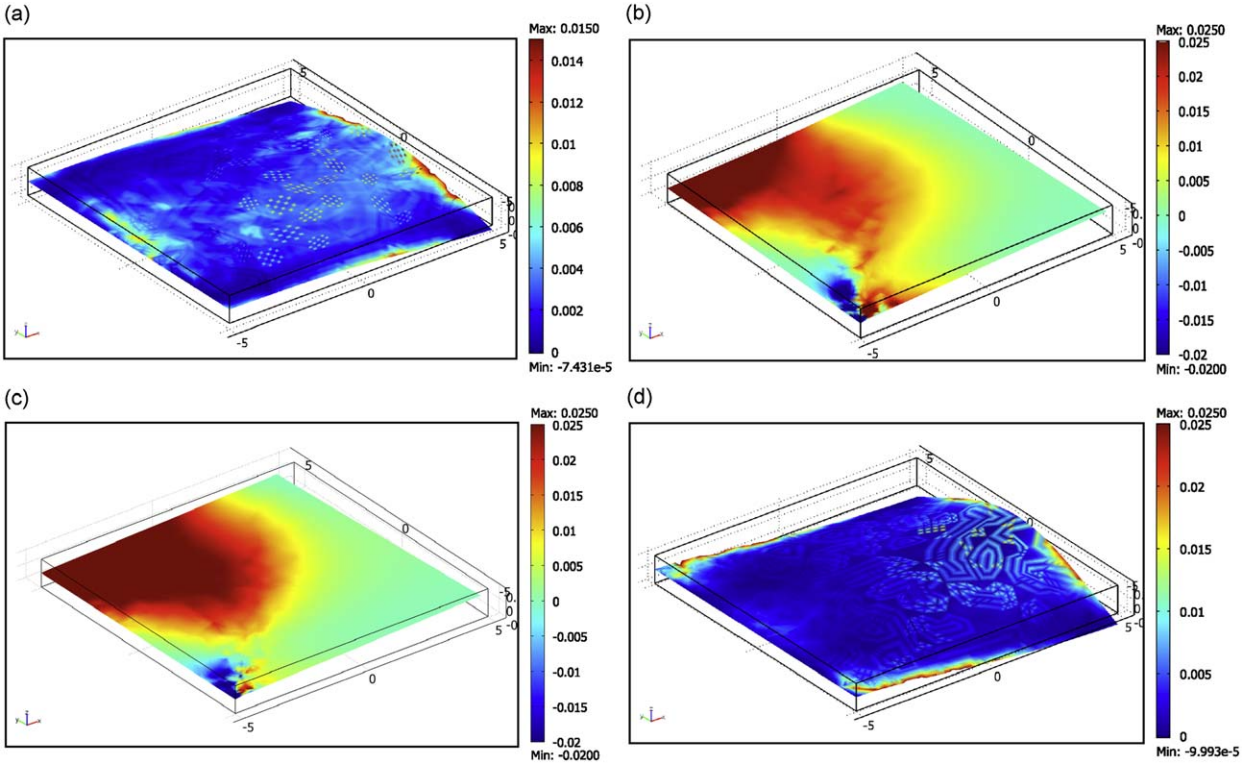

Fig. 10. Slices of the contour plots of the quasi-distortional stored-energy function associated with modes possessing closely spaced frequencies in an epoxy-based composite plate: (a)–(d) refer to the same modes depicted in Fig. 9. For the sake of clarity, the ranges in plots (b) and (c) were bounded with respect to the actual ranges of $[-0.3, 0.144]$ and $[-0.259, 0.22]$, respectively.

shows that it is not proportional to the spherical part of the stress (average normal stress). Thus the uncoupled form of the constitutive equations holds only for particular values of the elastic coefficients, even by incorporating all the expected simplifications ensuing from orthotropic symmetries.

To overcome this problem and investigate some aspects of the purely deviatoric component associated with the modal stresses, we calculated the von Mises stress of selected modes. We observe in Fig. 8 that the enhanced elastic properties of the composite materials are emphasised by the fact that the stored energy of the composite with longitudinally aligned CNTs is about five times larger than the energy in the pure matrix and the spatial pattern is similar. If we consider different alignments, the energy can be more uniformly distributed or can be localised although at the price of higher local peaks.

The analysis of the contour plots of the von Mises stress, associated with modes possessing closely spaced frequencies in epoxy-based CNT-reinforced composites, shows in Fig. 9 that, for longitudinally aligned CNTs, the third mode would vibrate with the same frequency as that of the fifth mode of the all-matrix plate. The von Mises stress distribution would not be very different in the CNT-reinforced case although it exhibits higher values due to the higher stiffness. The quasi-distortional stored-energy function, calculated in the same conditions as above, shows in Fig. 10 a confirmation of a close correlation between the deviatoric state of stress manifested through the von Mises stress states and the quasi-distortional stored energy.

Similar considerations can be made when comparing the mode shapes and the associated von Mises stresses of the composite plates made of different hosting matrices (see Figs. 11 and 12). In particular, an interesting result highlighted by the computations related to concrete-based composite plates is that the low-order modes, possessing frequencies close to that of the fourth mode of pure concrete, do exhibit lower modal von Mises stresses; in some configurations, these stresses are even lower than 50 percent.

7. Summary and conclusions

In this work, we have investigated carbon nanotube-reinforced composites in terms of linear elastic and vibrational properties, employing an equivalent continuum formulation based on the Eshelby–Mori–Tanaka approach. Such an approach, also known as the equivalent inclusion-average stress method, consists of the combination of the equivalent inclusion idea of Eshelby with the concept of average stress and strain in the isotropic elastic matrix of Mori and Tanaka. The elastic inclusions are assumed to be bonded to the matrix through a perfect interface.

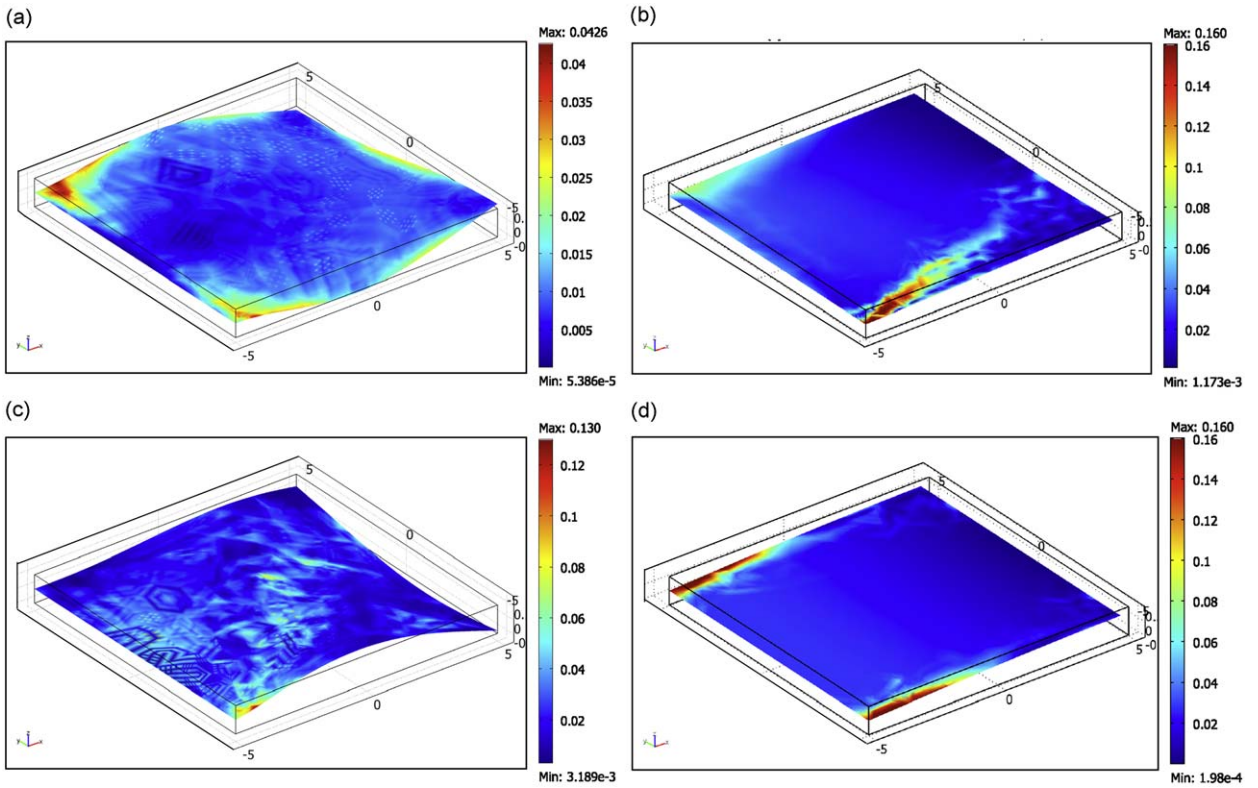

Fig. 11. Slices of the contour plots of the von Mises stress associated with modes possessing closely spaced frequencies in a rubber (Ru) composite plate: (a) 6th mode of the all-matrix plate, (b) 3rd mode of the nano-composite plate with $\phi = 5\pi/12$, (c) 3rd mode of the nano-composite plate with $\phi = \pi/4$, and (d) 3rd mode of the nano-composite plate with $\phi = \pi/2$.

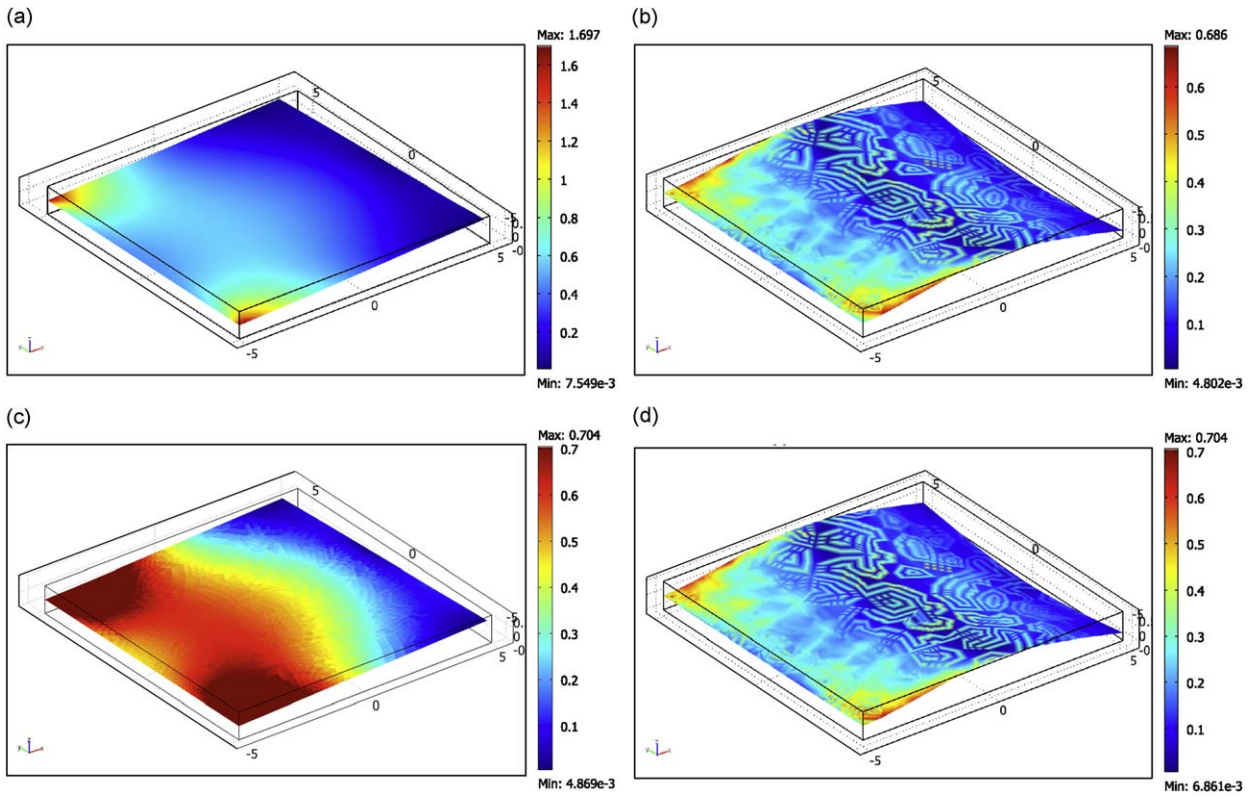

Fig. 12. Slices of the contour plots of the von Mises stress associated with modes possessing close frequencies in a concrete (Be) composite plate: (a) 4th mode of the all-matrix plate, (b) 3rd mode of the nano-composite plate with $\phi = 5\pi/12$, (c) 4th mode of the nano-composite plate with $\phi = \pi/6$, and (d) 3rd mode of the nano-composite plate with $\phi = \pi/2$. For the sake of clarity, the bounds in plot (c) were restricted from the actual range of $[4.869e^{-3}, 1.943]$.

The obtained elastic properties have proved to be very close to those registered through careful experimental measurements reported in the literature. In agreement with previous theoretical studies, reinforcement with carbon nanotubes is clearly capable of enhancing the longitudinal Young modulus of nano-composites. The improvement in performance is a function of alignment, volume fraction of nanotubes, and the type of matrix material. With respect to the pure uniform matrix, such an improvement achieves a maximum when the carbon nanotubes are uniformly aligned with the loading direction and the difference between the elastic modulus of the matrix and that of the carbon nanotubes is the highest.

The investigations into the modal properties, confined to the analysis of the lowest 10 modes of cantilevered composite plates, have shown that the integration of carbon nanotubes into the hosting material is indeed a powerful mechanism for tuning the vibrational properties of the composite plates. The fundamental frequency of CNT-reinforced plates can increase by nearly 500 percent, without practically altering the mass density of the material. In particular, the plates can be designed so as to respond with a dominant selected mode to certain given excitations. Further, the probability of failure in the prevailing mode may be minimised since the distortional part of the vibrational modal energy can accordingly be modified through the nano-structure of the material. This study is the first step towards a nonlinear equivalent continuum modelling that can describe the dissipation at the interfaces between carbon nanotubes and the hosting matrix.

References

[1] L. Bokobza, Multiwall carbon nanotube elastomeric composites: a review, *Polymer* 48 (2007) 4907–4920.
[2] J.D. Eshelby, The determination of the elastic field of an ellipsoidal inclusion, and related problems, *Proceedings of the Royal Society A* 241 (1957) 376–396.
[3] J.D. Eshelby, The elastic field outside an ellipsoidal inclusion, *Proceedings of the Royal Society A* 252 (1959) 561–569.
[4] T. Mura, *Micromechanics of Defects in Solids*, second ed., Martinus Nijhoff, The Netherlands, 1987.
[5] M.E. Gurtin, *Configurational Forces as Basic Concepts of Continuum Physics*, Springer, New York, 2000.
[6] T. Mori, K. Tanaka, Average stress in matrix and average elastic energy of materials with misfitting inclusions, *Acta Metallurgica* 21 (1973) 571–574.
[7] S. Giordano, P.L. Palla, L. Colombo, Nonlinear elasticity of composite materials. Landau coefficients in dispersions of spherical and cylindrical inclusions, *The European Physical Journal B* 68 (2009) 89–101.
[8] C.H. Chen, C.H. Cheng, Effective elastic moduli of misoriented short-fiber composites, *International Journal of Solids and Structures* 33 (1996) 2519–2539.

[9] G.M. Odegard, T.S. Gates, K.E. Wise, C. Park, E.J. Siochi, Constitutive modeling of nanotube-reinforced polymer composites, *Composites Science and Technology* 63 (2003) 1671–1687.
[10] Y. Benveniste, A new approach to the application of Mori–Tanaka's theory in composite materials, *Mechanics of Materials* 6 (1987) 147–157.
[11] G. Formica, W. Lacarbonara, Eshelby-like equivalent continuum modeling of carbon nanotube-based composite, *Proceedings of ESMC 2009, 7th EUROMECH Solid Mechanics Conference*, Lisbon, September 2009.
[12] V. Anumandla, R.F. Gibson, A comprehensive closed form micromechanics model for estimating the elastic modulus of nanotube-reinforced composites, *Composites: Part A* 37 (2006) 2178–2185.
[13] R.F. Gibson, E.O. Ayorinde, Y-F Wen, Vibrations of carbon nanotubes and their composites: a review, *Composites Science and Technology* 67 (2007) 1–28.
[14] P.M. Ajayan, J. Suhr, N. Koratkar, Utilizing interfaces in carbon nanotube reinforced polymer composites for structural damping, *Journal of Materials Science* 41 (2006) 7824–7829.
[15] H. Rajoria, N. Jalili, Passive vibration damping enhancement using carbon nanotube-epoxy reinforced composites, *Composites Science and Technology* 65 (2005) 2079–2093.
[16] B. Ashrafi, P. Hubert, Modeling the elastic properties of carbon nanotube array/polymer composites, *Composites Science and Technology* 66 (2006) 387–396.
[17] Y.H. Zhao, G.J. Weng, Effective elastic moduli of ribbon-reinforced composites, *Journal of Applied Mechanics* 57 (1990) 158–167.
[18] I. Schmidt, D. Gross, The equilibrium shape of an elastically inhomogeneous inclusion, *Journal of the Mechanics and Physics of Solids* 45 (1997) 1521–1549.
[19] I. Schmidt, D. Gross, Directional coarsening in Ni-based model for an elasticity base superalloys: analytical results, *Proceedings of the Royal Society A* 455 (1999) 3085–3106.
[20] S. Nemat-Nasser, M. Hori, *Micromechanics: Overall Properties of Heterogeneous Materials*, North-Holland Series in Applied Mathematics and Mechanics, 1993.
[21] B. Johannesson, O.B. Pedersen, Analytical determination of the average Eshelby tensor for transversely isotropic fiber orientation distributions, *Acta Materialia* 46 (1998) 3165–3173.
[22] J. Che, W. Yuan, G. Jiang, J. Dai, S.Y. Lim, M.B. Chan-Park, Epoxy composite fibers reinforced with aligned single-walled carbon nanotubes functionalized with generation 0–2 dendritic poly(amidoamine), *Chemistry of Materials* 21 (2009) 1471–1479.
[23] A. Allaoui, S. Bai, H.M. Cheng, J.B. Bai, Mechanical and electrical properties of a MWNT/epoxy composite, *Composites Science and Technology* 62 (2002) 1993–1998.
[24] M. Zheng, J. Yang, Z. Jin, Estimation of yield strength for composites reinforced by grains, *International Journal of Fracture* 68 (1994) 53–56.